photonics

MDPI

Article

Correlated Photon Lidar Based on Time-Division Multiplexing

Yun Jiang [1,2,3], Bo Liu [1,2,3,*], Zixun Wang [1,2,3,4], Fengyun Huang [1,2,3], Taibei Liu [1,2,3,4], Lan Luo [1,2,3], Feifan He [1,2,3], Yongqi Yang [1,2,3,4] and Bin Zhao [1,2,3]

1 National Laboratory on Adaptive Optics, Chinese Academy of Sciences, Chengdu 610209, China; jiangyun@ioe.ac.cn (Y.J.); wangzixun23@mails.ucas.edu.cn (Z.W.); huangfy@ioe.ac.cn (F.H.); liutaibei23@mails.ucas.edu.cn (T.L.); luolan@ioe.ac.cn (L.L.); hefeifan@ioe.ac.cn (F.H.); yangyongqi23@mails.ucas.ac.cn (Y.Y.); zhaobin@ioe.ac.cn (B.Z.)
2 Key Laboratory of Science and Technology on Space Optoelectronic Precision Measurement, Chinese Academy of Sciences, Chengdu 610209, China
3 Institute of Optics and Electronics, Chinese Academy of Sciences, Chengdu 610209, China
4 University of Chinese Academy of Sciences, Beijing 100049, China
* Correspondence: boliu@ioe.ac.cn

Abstract: Single-photon lidar (SPL) exhibits high sensitivity, making it particularly suitable for detecting weak echoes over long distances. However, its susceptibility to background noise necessitates the implementation of advanced filtering techniques and complex algorithms, which can significantly increase system cost and complexity. To address these challenges, we propose a time-division-multiplexing-based correlated photon lidar system that employs a narrowband pulsed laser with stable time delays and variable pulse intensities, thereby establishing temporal and intensity correlations. This all-fiber solution not only simplifies the system architecture but also enhances operational efficiency. An adaptive cross-correlation method incorporating time slicing has been developed to extract histogram signals, enabling successful 1.5 km distance measurements under intense daytime noise conditions, using a 1 s accumulation time and a 20 mm receiving aperture. The experimental results demonstrate a 38% (from 1.11 to 1.52) improvement in the signal-to-noise ratio (SNR), thereby enhancing the system's anti-noise capability, facilitating rapid detection, and reducing overall system costs.

Keywords: photon lidar; time-division multiplexing; ranging

Received: 6 January 2025
Revised: 24 January 2025
Accepted: 26 January 2025
Published: 27 January 2025

Citation: Jiang, Y.; Liu, B.; Wang, Z.; Huang, F.; Liu, T.; Luo, L.; He, F.; Yang, Y.; Wang, Z. Correlated Photon Lidar Based on Time-Division Multiplexing. *Photonics* **2025**, *12*, 114. https://doi.org/10.3390/photonics12020114

1. Introduction

Single-photon lidar (SPL) refers to a novel type of lidar that combines single-photon detection with high-precision time measurement technology. SPL exhibits exceptionally high detection sensitivity, capable of detecting weak energy at the single-photon level. It is currently widely applied in fields such as active remote sensing, long-distance target detection, and autonomous driving [1–9]. However, due to the inherent detection mechanism of single-photon detectors, these devices respond to all photons reaching the detector surface, and are unable to distinguish between signal and noise photons. This makes SPL highly susceptible to noise interference, leading to degraded performance under high-noise conditions [10]. In our prior research [11], it was established that intense background light during the day is the predominant factor influencing radar detection performance. While precipitation and fog can also impede laser detection, these effects can be partially mitigated. Additionally, the complexity of the SPL system necessitates the use of high-performance spectral filtering devices for background light suppression, which are costly and increase the overall system cost. These factors collectively constrain the broader application of SPL systems.

To address these challenges, researchers have explored various approaches to enhancing the operational capability of SPL [12,13]. One of the most effective methods is to suppress background noise through spectral filtering [14]. For instance, narrowband filters are commonly used for this purpose. However, the filtering bandwidth of current mainstream spectral filtering techniques is typically on the nanometer scale, which may not fully meet the stringent requirements of SPL systems. Signal encoding techniques have also been employed [15–18], where laser output pulses are encoded using programmable logic control devices to impart specific distributions to the signal light [19]. Representative methods include true or pseudo-random coding to improve the anti-interference capability of the signal [20]. In 2022, Wu et al. introduced a multi-beam single-photon light detection and ranging (LiDAR) system that achieves three-dimensional imaging at a distance of 75 m using a hybrid wavelength and time multiplexing technique at 1550 nm. The accumulation time for a single data point is 1 s [16]. In the same year, Zang et al. presented a system that integrates an all-optical encoder with a wavelength-division multiplexing (WDM) device to perform spectral and temporal coding on the illuminating light, enabling high-speed detection over a distance of 25 m [21]. However, these systems exhibit increased complexity, impose stringent requirements for beam control, and achieve relatively limited detection ranges. Upgrading hardware components, such as increasing the emission power or receiving aperture, has also been considered to boost detection capabilities [22]. However, these approaches further escalate system costs.

In this paper, we proposed a time-division-multiplexing-based correlated photon lidar scheme. This approach involves emitting multiple narrowband pulse sequences with fixed time delays from a pulsed laser. Each pulse sequence has varying intensities, providing both intensity and time correlations within the signal itself, without requiring external modulation. A single-photon detector is employed to simultaneously detect multiple pulses, significantly simplifying the lidar system architecture. We introduce a novel adaptive cross-correlation method for extracting signals from the photon accumulation histogram. Our experimental results demonstrate successful 1.5 km distance detection during periods of intense daytime background noise, with an accumulation time of only 0.5 to 1 s. To further enhance the signal-to-noise ratio (SNR) under strong background noise conditions, we propose a time-slicing method for individual measurements. This scheme effectively streamlines the system structure, reduces costs, and expands the potential application scenarios of single-photon lidar.

2. Methods

Current single-photon lidar primarily utilizes the time-of-flight (*TOF*) method. Through high-precision time measurement approaches, the flight time of photons emitted by the laser and reflected by the target is recorded, thereby obtaining the distance of the target. Herein, d represents the distance of the target, t denotes the flight time of the photon, and c stands for the speed of light, so $d = ct/2$. From the above equation, it can be concluded that the measurement accuracy of single-photon lidar solely depends on the timing accuracy of the system. Time-correlated single-photon counting (TCSPC) [23], featuring timing accuracy as low as the ps or even sub-ps level, is currently widely employed in domains such as the time measurement of single-photon lidar and fluorescence lifetime measurement. Single-photon detection is essentially probabilistic in nature. The echo signal is extremely feeble, with a very small number of photons or even no photons returning for each emitted pulse. The fundamental principle of TCSPC is shown in Figure 1, which is to continuously record the low-intensity, high-repetition-frequency echo photons reflected by the target. TCSPC accurately records the arrival time of each photon, accumulates it in a histogram to complete one count, and then, through multiple detections and accumulations,

photons with different arrival times are distributed and accumulated at different positions in the histogram. There are multiple time bins (Time bin) in the histogram, and the width of each time bin constitutes the time resolution of the detection, typically in the ps range. The total count in each time bin corresponds to the counting intensity at this position, and the original waveform of the signal can be derived by analyzing the histogram. It should be noted that the count value in the histogram cannot precisely reflect the number of photons, as the time resolution of the histogram directly affects the total count in each time bin.

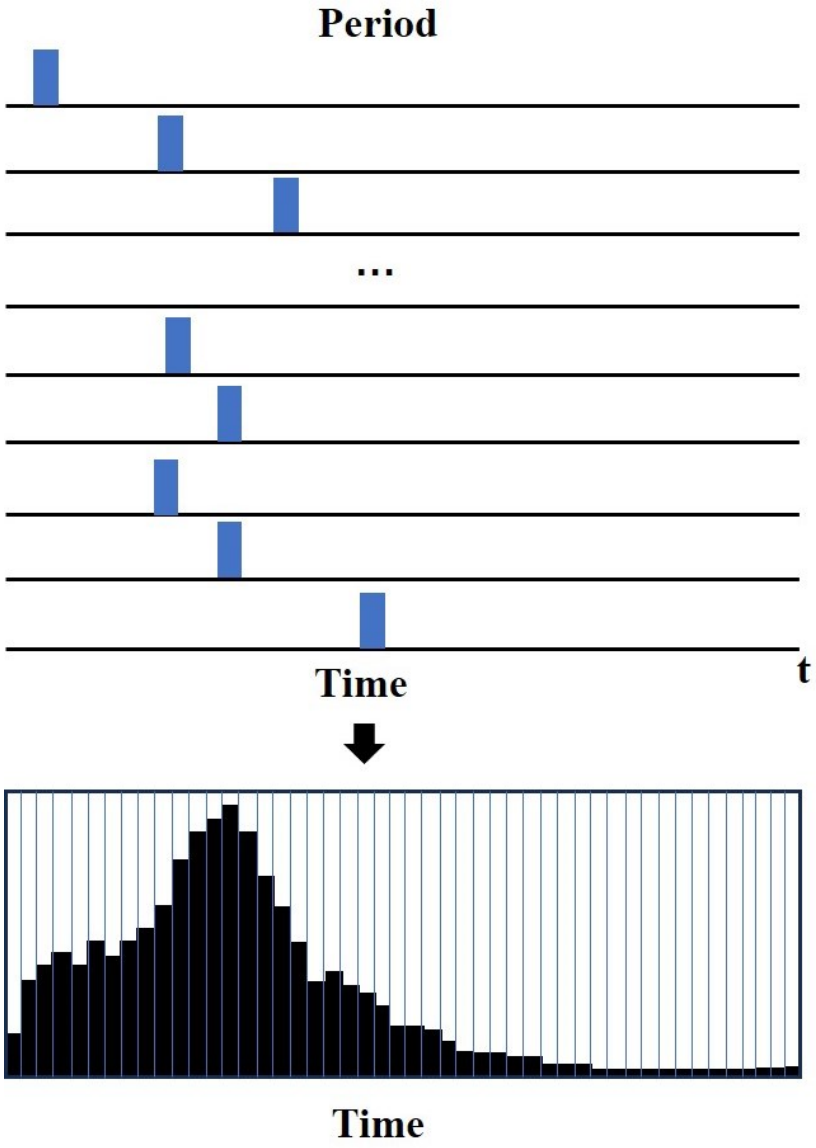

Figure 1. Schematic illustration of the TCSPC principle.

By analyzing the temporal positions corresponding to the peaks in the photon counting histogram, precise distance information of the target can be obtained. In the context of target ranging, the system relies solely on the signals within the histogram for distance measurement, and cannot leverage spatial correlation methods similar to those used in three-dimensional imaging to extract additional information. In a high-noise daytime environment, weak echo signals from distant targets are likely to be obscured by background noise, making them difficult to distinguish. While spectral filtering using band-pass filters can effectively reduce background noise levels, the fabrication of narrowband, high-transmittance filters is both technically challenging and expensive. Therefore, we propose a time-division-multiplexing-based correlated photon lidar scheme. This approach simulta-

neously emits and receives multiple pulse sequences with varying relative intensities to provide intensity correlation, and introduces time correlation through fixed time delays between pulses. By combining intensity and time correlations, the signal's resistance to interference is significantly enhanced, thereby improving the overall detection performance of the system.

In typical single-photon lidar systems that employ the time-of-flight (ToF) method for distance measurement, the primary approach to distinguishing signals from noise is by exploiting the distinct temporal distributions of target echoes and background noise echoes. Specifically, since the emitted laser pulse typically follows a Gaussian profile, the signal echo also adheres to a Gaussian distribution. In contrast, background noise exhibits random temporal distribution without any significant clustering characteristics. Consequently, the signal echo demonstrates a higher degree of temporal concentration compared to the noise signal. Signal extraction is achieved by leveraging these differences in the distribution characteristics of the signal and noise, as illustrated in Figure 2a.

However, in high-noise environments, most time bins are likely to be occupied by noise, leading to a considerable degree of noise aggregation. Additionally, the dead-time effect of single-photon detectors causes them to become temporarily unresponsive after detecting a photon. These factors collectively result in the inability to effectively separate target echo photons from background noise using simple clustering methods alone. As shown in Figure 2b, in strong noise conditions, the signal cannot be reliably extracted from the background noise solely through the aforementioned approach.

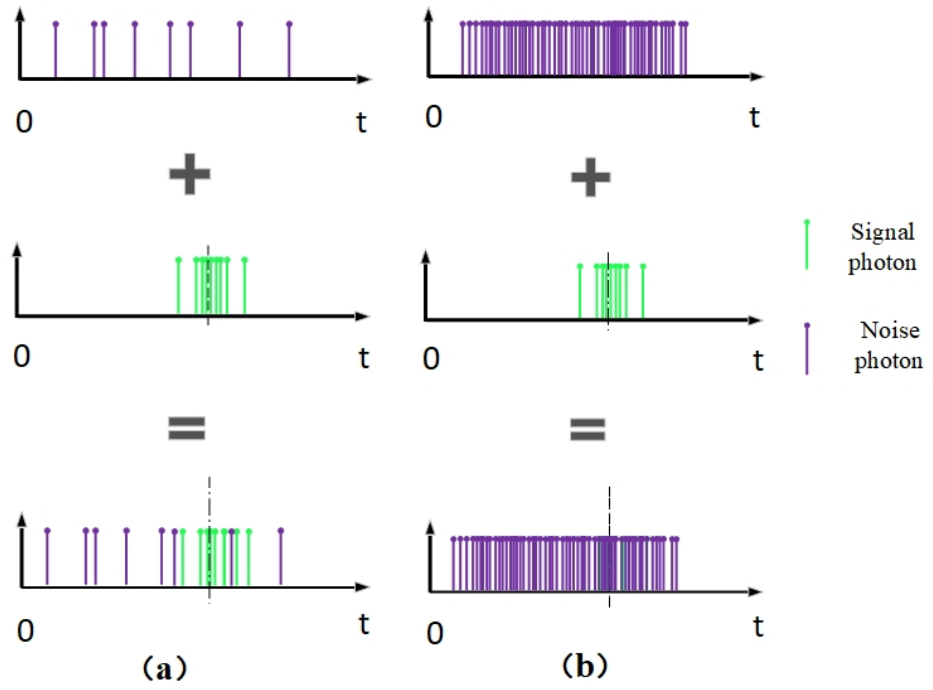

Figure 2. Photon distribution of echo signals under different noise intensities: (**a**) photon distribution under low-noise conditions; (**b**) photon distribution under high-noise conditions.

To address the challenge of target signals being obscured by background noise in a high-noise environment, where simple aggregation methods fail to effectively extract the signal, this paper proposes a time-division multiplexing correlated photon lidar system. Additionally, an "adaptive cross-correlation" method is introduced for extracting target signals in strong noise environments. The proposed method consists of two key steps. First, the single-photon lidar system emits multiple pulses with a fixed time delay. An adaptive template for each calculation is then derived from the single-shot measurement of the target

photon ranging histogram, which captures both the intensity and time delay information of the end-face reflection signal. In the second step, an adaptive cross-correlation operation is performed between the entire histogram and the adaptive template obtained from the current measurement, yielding the system's adaptive correlation function. By identifying the extremum of this function, the target signal, which was previously masked by background noise, can be effectively extracted. Among them, the adaptive template can be expressed as $T_p(t)$, where

$$T_p(t) = \begin{cases} \alpha_1 & t = t_i \\ \alpha_2 & t = t_i + \Delta t \end{cases} \tag{1}$$

The relative intensities of the two pulses in the template $T_p(t)$ are represented by α_1 and α_2, respectively, which reflect the intensity correlation of the two signal pulses. t_i represents the time corresponding to the adaptive pulse template, and Δt represents the fixed delay between the two pulses in the template, providing the temporal correlation of the signal. The echo photon counting histogram is a discrete time series, $T_{hist} = \{t_1, t_2, \ldots, t_n\}$, abbreviated as T_h , where t_n represents the flight time of each photon. t_p and t_{hist} represent two sets of random signals, and the degree of correlation between the two signals is defined by the following equation:

$$R(T_p(t), T_{hist}(t)) = E(T_p(t) * T_{hist}(t)) \tag{2}$$

As both of the above-mentioned signals are discrete time variables, it follows that

$$(T_p * T_h)(n) = \sum_{t_0}^{t_n} T_p(n) * T_h(n+m) \tag{3}$$

In the aforementioned Equation (3), n represents the initial position for the calculation of the two sequences, m represents the sliding amount of each sequence, t_0 represents the initial time position of the time sequence, and t_n represents the end time of the time sequence. It can be set as

$$C_{ACC}(t) = (T_p * T_h)(n) \tag{4}$$

In the above Equation (4), the adaptive cross-correlation function, denoted by $C_{ACC}(t)$, can be calculated based on the photon flight time at the extremum of the function to obtain the target distance:

$$Z = \frac{\max(C_{ACC}) \cdot c}{2} \tag{5}$$

In Equation (1), $T_p(t)$ is the adaptive template obtained from the histogram sequence, which solely depends on the current measurement outcome. Therefore, it can reflect the mutual relationship between single signals with greater precision. Essentially, it is a cross-correlation operation performed on two vectors. Figure 3a presents the distribution of signals and noise in a situation of high noise and multiple pulses. As depicted in Figure 3b, α_1 and α_2, respectively, represent the intensity information of the two pulses obtained through end-face reflection (derived from the histogram sequence of actual measurements), which reflects the intensity correlation of the emission pulses. Δt is the time delay between the two pulses, corresponding to the time difference of the emission pulses and providing the temporal correlation of the signal. Due to the fact that single-photon detection is of a probabilistic nature, there exist minute temporal variances among the emitted lasers for

each emission. Consequently, the convolution kernel templates obtained for each detection are not identical. Utilizing the measurement results of the current measurement as the convolution template can precisely reflect the correlation of the current measurement.

At the same time, the delay of the simultaneously emitted pulses is fixed and stable. Therefore, the delay of the target echo signal reflected back by the same target will also be fixed as Δt . Although the background noise is intense and it is impossible to obtain the target signal directly from the background noise, the signal still has a higher degree of aggregation than the noise, and there is no fixed time delay among the noise. Through this difference, the signal can be extracted from the noise. The adaptive template simultaneously provides the intensity-related information and temporal correlation of the target in the above process. The two-dimensional correlation can effectively guarantee the success rate of signal extraction.

It is important to emphasize that this method fundamentally differs from traditional signal encoding approaches. Conventional signal encoding techniques typically involve secondary control or modulation of the laser output using programmable logic controllers or similar devices, which can significantly increase system complexity and cost. Moreover, the relationships between encoded pulses in traditional methods are not consistent, complicating the processing and interpretation of individual test results.

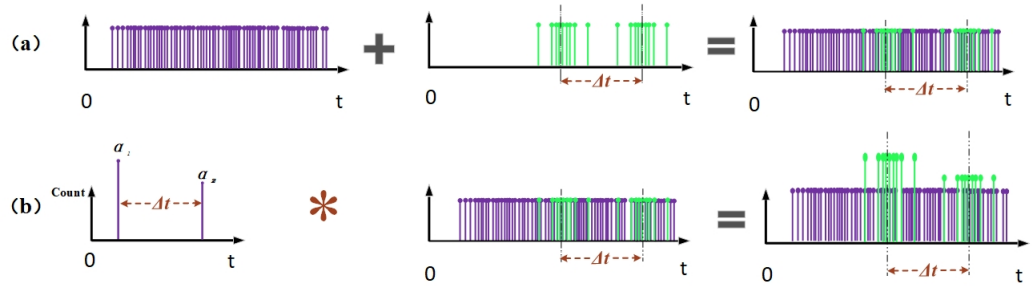

Figure 3. Adaptive cross-correlation processing method: (**a**) distribution of backscattered photons under double-delay pulses; (**b**) results processed by the * adaptive cross-correlation method.

3. System and Experiment

In anticipation of potential challenges during the actual deployment of the system, we have prioritized a simplified design by adopting an all-fiber structure, as illustrated in Figure 4. This configuration effectively mitigates optical path drift issues caused by vibration, overheating, and external environmental factors, thereby ensuring reliable signal reception. Furthermore, a single-fiber collimator is utilized to prevent signal loss due to misalignment between the receiving and transmitting fields of view when deploying the lidar. The time-division multiplexing function of the lidar is achieved through the use of a single laser and a single-pixel single-photon detector, which reduces the number of components and consequently lowers the overall system cost.

The correlated single-photon lidar system employs a custom laser that generates multiple delayed pulses centered at 1550 nm. Each pulse exhibits stable center wavelengths with a full width at half maximum (FWHM) of approximately 20 pm. Additionally, these laser pulses have fixed and consistent time delays and are emitted simultaneously. The laser pulse repetition rate is adjustable between 1 and 20 kHz, while the average output power can be tuned to approximately 80 mW. We are currently utilizing a single-pixel SPAD detector manufactured by IDQ, featuring an InGaAs/InP substrate and a pixel size of 16 microns. This detector supports both free-running and gated operation modes, with detection performed via fiber-optic coupling. The schematic diagram of the entire system is shown in Figure 4, and Table 1 summarizes the key system parameters.

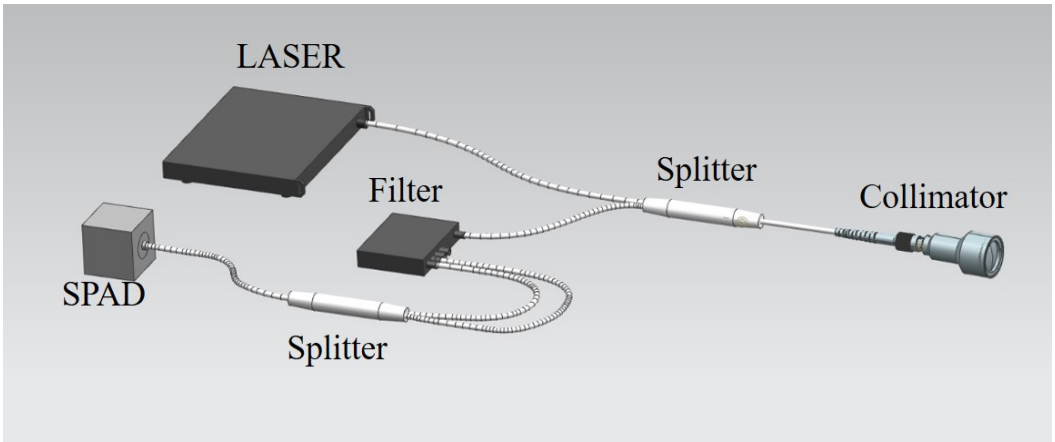

Figure 4. Schematic diagram of the correlated single-photon lidar system.

Table 1. Parameters of single-photon lidar system.

System Parameters	Parameters
Wavelength/nm	1550
Repetition frequency/kHz	20
Average output power/mw	80
Receiving aperture/mm	20

The system employs an all-fiber architecture, which significantly simplifies its design. A fiber collimator with a 20 mm aperture functions as both the transmitter and receiver telescope. The echo light is spectrally separated by a fiber filter, which also helps to mitigate background light noise. Pulsed light signals at different times are combined using a fiber combiner and subsequently detected by a single-photon detector. Initially, the output pulse timing sequence of the laser was characterized, as illustrated in Figure 5.

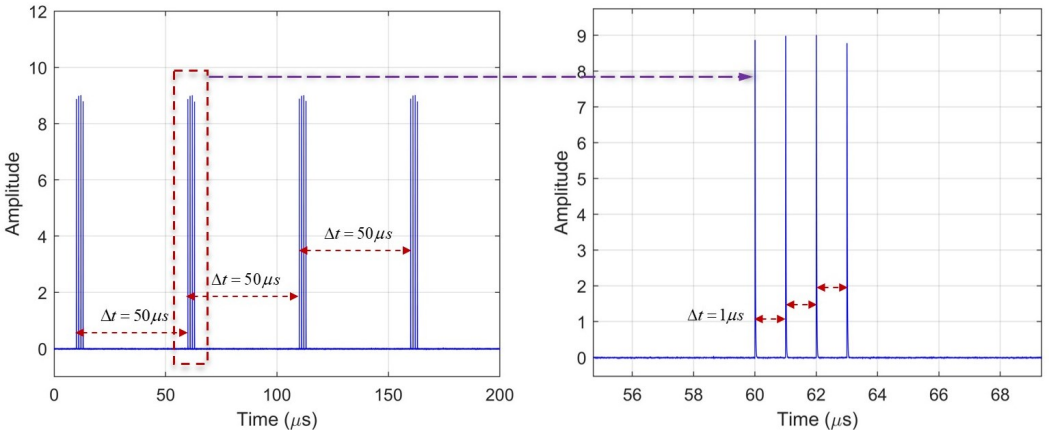

Figure 5. Timing diagram of the laser output pulse.

As shown in Figure 5, the laser exhibits four distinct output peaks, each corresponding to a unique time-delayed pulse, with a constant interval between consecutive pulses. Given the practical constraints of the experimental setup, two of these pulses were selected as test pulses during the experiment. The multiple outputs are time-division-multiplexed via time delays. The system is fully fiber-based, eliminating the need for complex optical path alignment and thereby reducing both system complexity and cost. Upon deployment, the system was tested for its ranging capability during the midday period, when solar background radiation was most intense. The system was positioned on an optical bench adjacent to a window, with a laser collimating mirror serving as both the transmitting and

receiving telescope. This configuration minimized energy loss due to potential misalignment between the transmit and receive fields of view and simplified system calibration. Distance measurements were performed on a building located approximately 1.5 km from the test site, with experiments conducted at various accumulation times. Figure 6 illustrates the experimental setup.

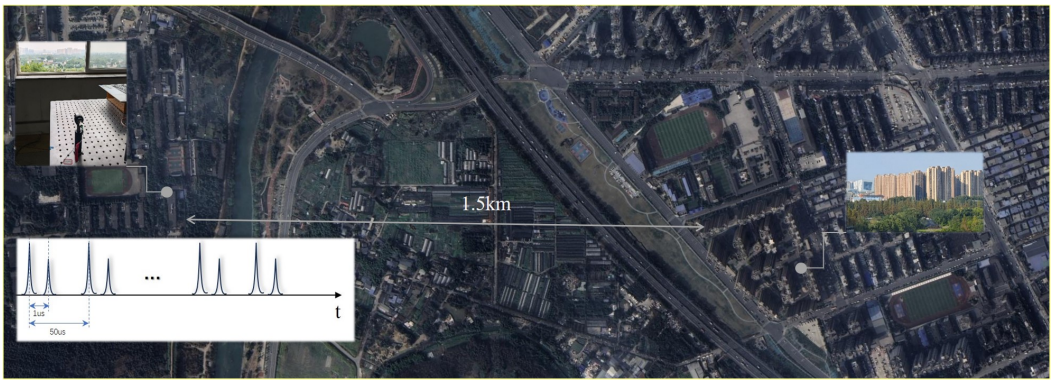

Figure 6. Schematic diagram of the experimental setup.

The total experiment duration was 1 s, with a system time resolution of 1 ns, corresponding to a distance resolution of 0.15 m. The single-shot ranging histogram is shown in Figure 7a. From the figure, it can be observed that the noise level is high near the target region, and a strong end-face reflection peak appears at short range. This peak is caused by the coupling between the output fiber end face and the laser beam expander lens. Traditional peak detection methods or simple cross-correlation approaches are ineffective in this scenario. The single-point ranging method lacks the capability to provide additional spatial correlation, which is essential for enhancing the system's signal-to-noise ratio. For the peak detection method, determining the target distance solely by identifying the peak of the photon count histogram becomes unreliable in high-noise environments, making it challenging to accurately ascertain the target position. The cross-correlation method, which involves performing cross-correlation between the original laser pulse waveform and the photon count histogram sequence, also proves ineffective under high-noise conditions, as illustrated in Figure 7c. Moreover, the time jitter of the laser pulse can introduce instability into time measurements. However, this effect can be mitigated by accumulating multiple SPL measurements, while reducing the laser pulse width can further diminish its impact. Additionally, the inherent dark count and dead time of the detector are unavoidable sources of noise that can only be minimized through the development of detectors with superior performance.

However, the adaptive cross-correlation method described earlier utilizes these two peaks as adaptive templates for calculation and then performs cross-correlation operations with the photon histogram sequence of the target area to obtain the target signal. In the enlarged view of the original histogram, multiple peaks exist, making it difficult to determine the position of the target echo. After applying the adaptive cross-correlation method once, the result, as shown in Figure 7b, clearly identifies the echo signal at 1550 m.

As the background noise intensity further increases, the single adaptive method is likely to become ineffective due to the extremely low signal-to-noise ratio (SNR). To address this issue, a time-splitting slice method was proposed. This method leverages the more dispersed and random nature of noise by dividing the 1 s cumulatively ranging experiment into five separate 0.2 s intervals. In each interval, the target signal remains in the same position within the time series, while the distribution of background noise varies independently across intervals. By performing independent adaptive cross-correlation

calculations on the accumulated data from each 0.2 s segment and then summing the results of the five intervals, the target signal can be effectively restored.

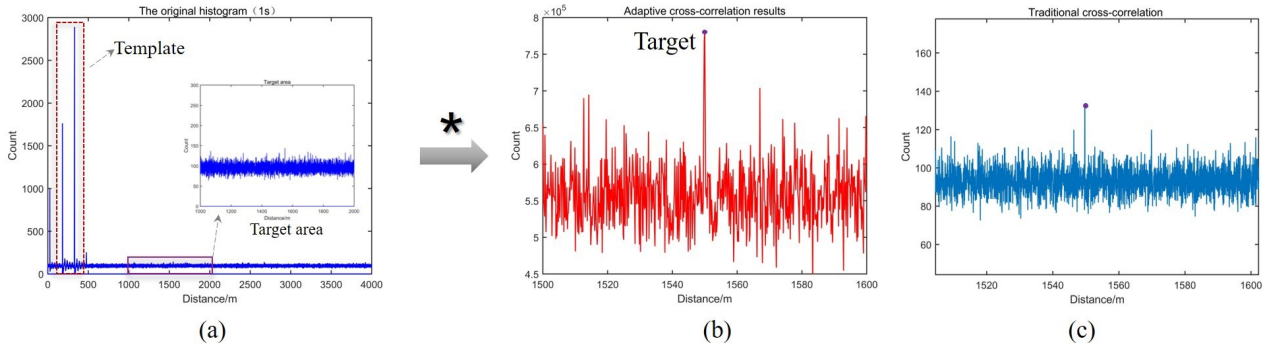

Figure 7. Schematic diagram of the experimental setup: (**a**) original ranging histogram; (**b**) results obtained via adaptive cross-correlation method; (**c**) traditional cross-correlation result. The * represents the adaptive cross-correlation operation.

The entire process is as follows: after processing the 1 s accumulation test results using the adaptive cross-correlation method, a "double-peak phenomenon" emerged, making it difficult to accurately determine the position of the signal echo, as shown in Figure 8a. However, by applying the time-splitting slice method described above, the target echo signal can be successfully recovered within the same accumulation time, and the "double-peak phenomenon" is eliminated. The specific calculation process is illustrated in Figure 8b, where ①–⑤ represent the results after each 0.2 s accumulation, and Figure 8c shows the final recovery result.

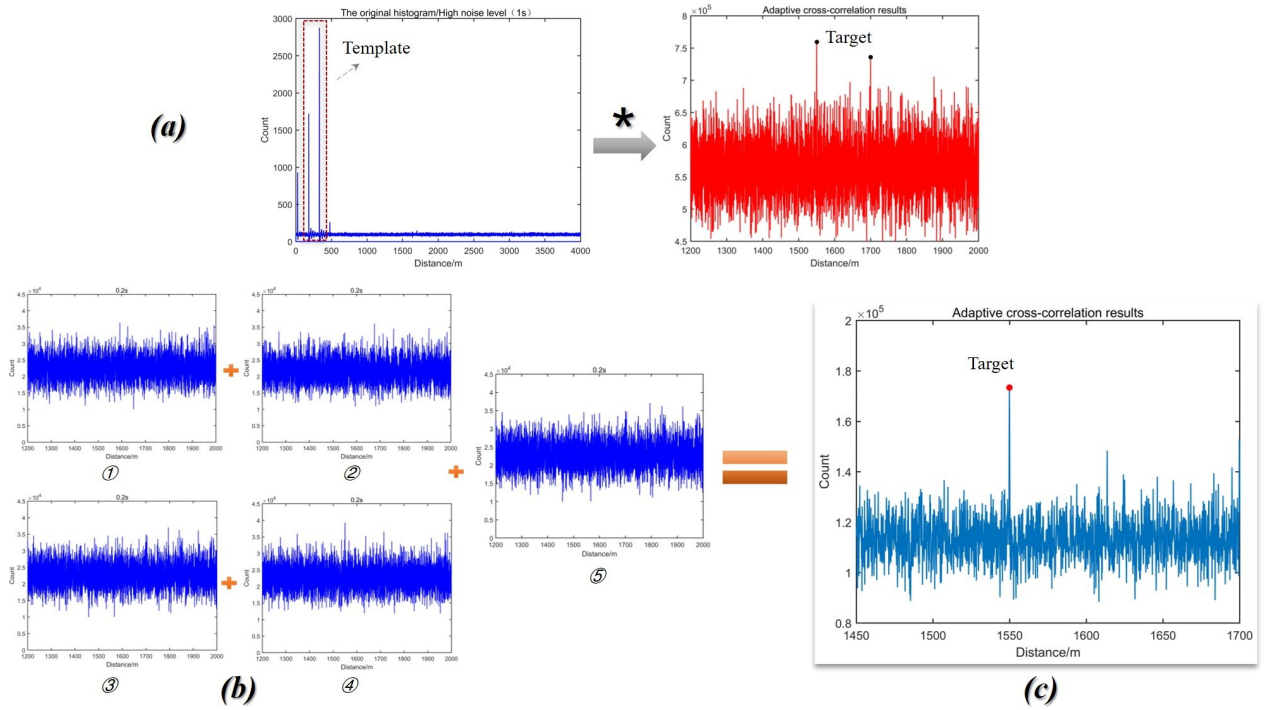

Figure 8. The time-splitting slicing method successfully restores the target signal. (**a**) The original 1 s accumulated signal exhibits a bimodal phenomenon after adaptive cross-correlation processing. The * represents the adaptive cross-correlation operation. (**b**) Accumulation of five groups of 0.2 s time slices, where ①–⑤ represent the results from each 0.2 s segment. (**c**) The final recovery result using the time-splitting slicing method.

Furthermore, we also examine the signal-to-noise ratios of various methods, as detailed in Table 2 below.

Table 2. Comparison of signal-to-noise ratio of different methods.

Method	SNR
Peak value method	1.11
Cross-correlation method	1.33
One-time adaptive cross-correlation method	1.42
Time-splitting slice method	1.52

From the experimental results presented, it is evident that the correlated photon lidar system based on time-division multiplexing (TDM) provides enhanced temporal and intensity correlations compared to traditional single-pulse emission systems. When combined with the proposed adaptive cross-correlation method, this system can successfully restore histogram signals to a distinguishable state in high-noise and low-accumulation-time scenarios, where traditional methods fail. Furthermore, a time-slicing technique has been introduced to address high-noise environments. By dividing the measurement into multiple short time intervals, the target signal can be effectively recovered within the same total accumulation time. Compared to the currently prevalent peak detection method and cross-correlation method, the proposed approach achieves a significantly higher signal-to-noise ratio (SNR). Specifically, the SNR has increased from 1.11 in the peak method to 1.52, representing a 38% improvement. The simplicity of the system structure and the elimination of complex hardware filtering requirements offer significant advantages for the practical application of single-photon lidar. Given that the optical path employs a coaxial transceiver configuration, only a simple scanning mechanism is needed to achieve long-distance three-dimensional imaging, which will be the focus of future work. This design broadens the potential applications of the system.

4. Conclusions

In this paper, we introduce a time-division-multiplexed multi-dimensional correlated photon lidar system and propose an adaptive cross-correlation method for extracting echo signals. The system features a simplified structure implemented with an all-fiber configuration that significantly reduces system complexity and cost. By leveraging the intensity and temporal correlations provided by multiple pulses, we conducted a single-photon ranging experiment under intense background noise conditions during the daytime. Using the adaptive cross-correlation method, the signal was successfully recovered. For scenarios with high background noise, where a single adaptive cross-correlation is insufficient, we further developed a time-splitting slicing technique to enhance the performance of the adaptive cross-correlation approach, ultimately achieving successful recovery of the ranging signal. The signal-to-noise ratio was increased from 1.1 to 1.52 by the traditional peak method, which is an increase of 38%. The ranging experiment achieved a distance of 1.5 km with a total accumulation time of 1 s. This work demonstrates the operational effectiveness of the correlated single-photon lidar system and provides new insights for optimizing system architecture, miniaturization for engineering applications, and improving detection performance in single-photon lidar systems.

Author Contributions: Conceptualization, Y.J. and B.L.; methodology, Y.J.; software, Z.W. and F.H. (Feifan He); validation, Y.J., T.L. and L.L.; resources, B.L.; data curation, Y.J. and Y.Y.; writing—original draft preparation, Y.J.; writing—review and editing, Y.J., B.Z. and B.L.; visualization, F.H. (Fengyun Huang). All authors have read and agreed to the published version of the manuscript.

Funding: This work was supported by the National Natural Science Foundation of China (Grant No.: 62375266).

Data Availability Statement: Data will be supplied as required.

Conflicts of Interest: The authors declare no conflicts of interest.

Abbreviations

The following abbreviations are used in this manuscript:

SPL	Single-photon lidar
TOF	Time of flight
TCSPC	Time-correlated single-photon counting

References

1. Chen, Z.; Fan, R.; Li, X.; Dong, Z.; Zhou, Z.; Ye, G.; Chen, D. Accuracy improvement of imaging lidar based on time-correlated single-photon counting using three laser beams. *Opt. Commun.* **2018**, *429*, 175–179. [CrossRef]
2. Pawlikowska, A.M.; Halimi, A.; Lamb, R.A.; Buller, G.S. Single-photon three-dimensional imaging at up to 10 km range. *Opt. Express* **2017**, *25*, 11919–11931. [CrossRef] [PubMed]
3. Du, B.; Pang, C.; Wu, D.; Li, Z.; Peng, H.; Tao, Y.; Wu, E.; Wu, G. High-speed photon-counting laser ranging for broad range of distances. *Sci. Rep.* **2018**, *8*, 4198. [CrossRef] [PubMed]
4. Gariepy, G.; Krstajić, N.; Henderson, R.; Li, C.; Thomson, R.R.; Buller, G.S.; Heshmat, B.; Raskar, R.; Leach, J.; Faccio, D. Single-photon sensitive light-in-fight imaging. *Nat. Commun.* **2015**, *6*, 6021. [CrossRef]
5. Li, Z.P.; Ye, J.T.; Huang, X.; Jiang, P.Y.; Cao, Y.; Hong, Y.; Yu, C.; Zhang, J.; Zhang, Q.; Peng, C.Z.; et al. Single-photon imaging over 200 km. *Optica* **2021**, *8*, 344–349. [CrossRef]
6. Abdalati, W.; Zwally, H.J.; Bindschadler, R.; Csatho, B.; Farrell, S.L.; Fricker, H.A.; Harding, D.; Kwok, R.; Lefsky, M.; Markus, T.; et al. The ICESat-2 laser altimetry mission. *Proc. IEEE* **2010**, *98*, 735–751. [CrossRef]
7. Li, Y.; Ibanez-Guzman, J. Lidar for autonomous driving: The principles, challenges, and trends for automotive lidar and perception systems. *IEEE Signal Process. Mag.* **2020**, *37*, 50–61. [CrossRef]
8. Du, B.; Wang, Y.; Wu, E.; Chen, X.; Wu, G. Laser communication based on a multi-channel single-photon detector. *Opt. Commun.* **2018**, *426*, 89–93. [CrossRef]
9. Royo, S.; Ballesta-Garcia, M. An overview of lidar imaging systems for autonomous vehicles. *Appl. Sci.* **2019**, *9*, 4093. [CrossRef]
10. Sun, W.; Hu, Y.; MacDonnell, D.G.; Weimer, C.; Baize, R.R. Technique to separate lidar signal and sunlight. *Opt. Express* **2016**, *24*, 12949–12954. [CrossRef]
11. Bo, L.; Yun, J.; Rui, W.; Zhen, C.; Bin, Z.; Fengyun, H.; Yuqiang, Y. Technical progress and system evaluation of all-time single photon lidar. *Infrared Laser Eng.* **2023**, *52*, 20220748-1–20220748-15.
12. Zheng, T.; Shen, G.; Li, Z.; Yang, L.; Zhang, H.; Wu, E.; Wu, G. Frequency-multiplexing photon-counting multi-beam LiDAR. *Photonics Res.* **2019**, *7*, 1381–1385. [CrossRef]
13. Zhang, Z.; Zhao, Y. Noise filtering strategy in photon-counting laser radar using the multi-gates detection method. *Optik* **2016**, *127*, 8926–8932. [CrossRef]
14. Han, F.; Liu, H.; Sun, D.; Han, Y.; Zhou, A.; Zhang, N.; Chu, J.; Zheng, J.; Jiang, S.; Wang, Y. An ultra-narrow bandwidth filter for daytime wind measurement of direct detection Rayleigh lidar. *Curr. Opt. Photonics* **2020**, *4*, 69–80.
15. Zhao, Y.; Tian, Y.; Zhang, X.; Xie, M.; Hao, W.; Su, X. Analysis of coded dual-repetition rate single-photon LIDAR. *Opt. Commun.* **2025**, *574*, 131148. [CrossRef]
16. Wu, D.; Zheng, T.; Wang, L.; Chen, X.; Yang, L.; Li, Z.; Wu, G. Multi-beam single-photon LiDAR with hybrid multiplexing in wavelength and time. *Opt. Laser Technol.* **2022**, *145*, 107477. [CrossRef]
17. Wu, D.; Yang, L.; Chen, X.; Li, Z.; Wu, G. Multi-channel pseudo-random coding single-photon ranging and imaging. *Chin. Opt. Lett.* **2022**, *20*, 021202. [CrossRef]
18. Ren, X.; Altmann, Y.; Tobin, R.; Mccarthy, A.; Mclaughlin, S.; Buller, G.S. Wavelength-time coding for multispectral 3D imaging using single-photon LiDAR. *Opt. Express* **2018**, *26*, 30146–30161. [CrossRef]

19. Kim, G.; Park, Y. LIDAR pulse coding for high resolution range imaging at improved refresh rate. *Opt. Express* **2016**, *24*, 23810–23828. [CrossRef]
20. Liu, B.; Yu, Y.; Chen, Z.; Han, W. True random coded photon counting Lidar. *Opto-Electron. Adv.* **2020**, *3*, 190044. [CrossRef]
21. Zang, Z.; Li, Z.; Luo, Y.; Han, Y.; Li, H.; Liu, X.; Fu, H. Ultrafast parallel single-pixel LiDAR with all-optical spectro-temporal encoding. *APL Photonics* **2022**, *7*, 046102. [CrossRef]
22. Albota, M.A.; Heinrichs, R.M.; Kocher, D.G.; Fouche, D.G.; Player, B.E.; O'Brien, M.E.; Aull, B.F.; Zayhowski, J.J.; Mooney, J.; Willard, B.C.; et al. Three-dimensional imaging laser radar with a photon-counting avalanche photodiode array and microchip laser. *Appl. Opt.* **2002**, *41*, 7671–7678. [CrossRef] [PubMed]
23. Massa, J.S.; Wallace, A.M.; Buller, G.S.; Fancey, S.; Walker, A.C. Laser depth measurement based on time-correlated single-photon counting. *Opt. Lett.* **1997**, *22*, 543–545. [CrossRef] [PubMed]